Couplings of Microstrip Square Open-Loop Resonators for Cross-Coupled Planar Microwave Filters

Jia-Sheng Hong, *Member, IEEE,* and Michael J. Lancaster, *Member, IEEE*

Abstract— A new type of cross-coupled planar microwave filter using coupled microstrip square open-loop resonators is proposed. A method for the rigorous calculation of the coupling coefficients of three basic coupling structures encountered in this type of filters is developed. Simple empirical models are derived for estimation of the coupling coefficients. Experiments are performed to verify the theory. A four-pole elliptic function filter of this type is designed and fabricated. Both the theoretical and experimental performance is presented.

I. INTRODUCTION

MODERN microwave communication systems require, especially in satellite and mobile communications, high-performance narrow-band bandpass filters having low insertion loss and high selectivity together with linear phase or flat group delay in the passband. According to the early work on filter synthesis [1], it has been known that when frequency selectivity and bandpass loss are considered to be the important filtering properties, then the optimum filters are those exhibiting ripple in both passbands and stopbands. Such a filter response can be realized using filters with cross couplings between nonadjacent resonators [2]. These cross couplings give a number of alternative paths which a signal may take between the input and output ports. Depending on the phasing of the signals, the multipath effect may cause attenuation poles at finite frequencies or group delay flattening, or even both simultaneously. Usually, the cross-coupled resonator filters are realized using waveguide cavities or dielectric resonator loaded cavities because of their low loss. However, in order to reduce size, weight, and cost, there has been a growing interest in planar structures [3]–[14]. The disadvantage of high conductor loss of the planar filters using conventional conducting thin films can be overcome by replacing them with high-temperature superconducting (HTS) thin films. These can have a very low conductor loss [3]–[6]. An alternative is by combining with active MMIC devices to compensate the loss [14].

One difficulty in realizing the cross-coupled microwave filters in the planar structures is to identify and control the required electric and magnetic couplings for the nonadjacent
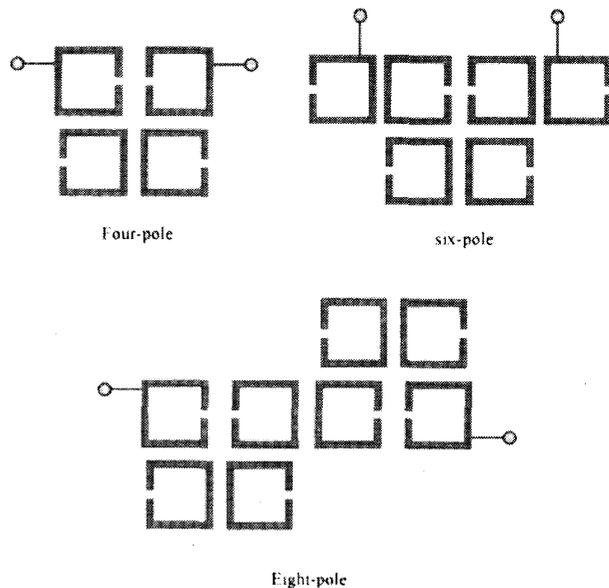
Fig. 1. Some cross-coupled planar microwave bandpass filters comprised of coupled microstrip square open-loop resonators on substrate (not shown) with a relative dielectric constant ε_r and a thickness h.

resonators. Several new cross-coupled planar filter structures have been proposed recently, including the microstrip dual-mode filters [3], [9], the dual-plane multicouple line filters [10] and the microstrip square open-loop resonator filters [13]. Shown in Fig. 1 are some typical cross-coupled planar filters comprised of microstrip square open-loop resonators. Compared with the microstrip dual-mode filters the microstrip square open-loop resonator filters can have a smaller size. For instance a four-pole dual-mode ring filter requires a circuit size amounting to $2\lambda_{go}/\pi \times \lambda_{go}/\pi$, where λ_{go} is the guided wavelength at the midband frequency. Whilst the circuit size for a four-pole open-loop resonator filter as shown in Fig. 1, only amounts to $\lambda_{go}/4 \times \lambda_{go}/4$, giving more than 50% size reduction. Compared with the dual-plane multicoupled line filters, the microstrip open-loop resonator filters are much simpler in structure, they require no grounding and coupling apertures. It would also seem that the coupled square open-loop resonators are more flexible to construct a variety of cross-coupled planar filters which have the similar coupling configurations as those of waveguide cavity cross-coupled filters.
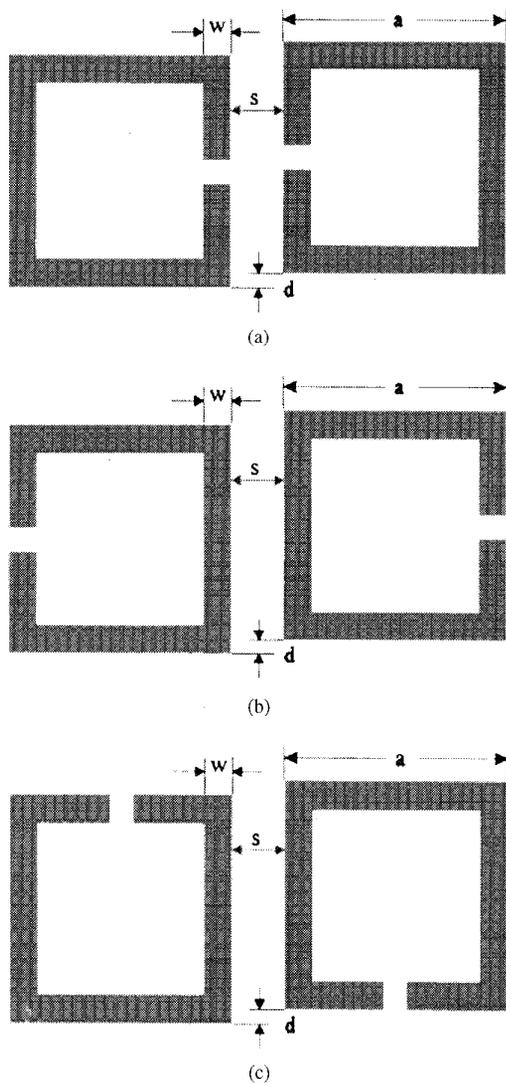
(a)

(b)

(c)

Fig. 2. Basic coupling structures of coupled microstrip square open-loop resonators on substrate (not shown) having a relative dielectric constant ε_r and a thickness h. (a) Electric coupling structure. (b) Magnetic coupling structure. (c) Mixed coupling structure.

derives the relationships that are necessary for extracting the coupling coefficients of the three basic coupling structures from the information of resonant mode splitting. In Section IV we present numerical results and deduce simple empirical models for estimation of the coupling coefficients. Experimental results are also presented to verify the theory. Section V demonstrates the filter application. A four-pole cross-coupled microstrip filter comprised of coupled square open-loop resonators is designed and fabricated. Theoretical and measured performance of the filter is presented. Conclusions are followed in Section VI.

II. COUPLING STRUCTURES

Shown in Fig. 2 are the three basic coupling structures encountered in the type of cross-coupled filters in Fig. 1. The coupled structures result from different orientations of a pair of identical square open-loop resonators which are separated by a spacing s and may or may not be subject to an offset d. It is obvious that any coupling in those coupling structures is that of the proximity coupling, which is, basically, through fringe fields. The nature and the extent of the fringe fields determine the nature and the strength of the coupling. It can be shown that at resonance, each of the open-loop resonators has the maximum electric field density at the side with an open-gap, and the maximum magnetic field density at the opposite side. Because the fringe field exhibits an exponentially decaying character outside the region, the electric fringe field is stronger near the side having the maximum electric field distribution, while the magnetic fringe field is stronger near the side having the maximum magnetic field distribution. It follows that the electric coupling can be obtained if the open sides of two coupled resonators are proximately placed as Fig. 2(a) shows, while the magnetic coupling can be obtained if the sides with the maximum magnetic field of two coupled resonators are proximately placed as Fig. 2(b) shows. For the coupling structure in Fig. 2(c), the electric and magnetic fringe fields at the coupled sides may have comparative distributions so that both the electric and the magnetic couplings occur. In this case the coupling may be referred to as the mixed coupling.

III. FORMULATION FOR COUPLING COEFFICIENTS

The physical mechanism underlying the resonant mode splitting is that the coupling effect can both enhance and reduce the stored energy. It has been pointed out that two resonant peaks in association with the mode splitting can be observed if the coupled resonator circuit are over-coupled, which occurs when the corresponding coupling coefficient is larger than a critical value amounting to $1/Q$, with Q the quality factor of the resonator circuit [17]. It is quite easy to identify in the full-wave EM simulation the two split resonant frequencies, which are related to the coupling coefficient. Hence the coupling coefficient can easily be determined if the relationships between the coupling coefficient and the resonant mode splitting are found. In what follows we present the formulation of such relationships for the coupled structures in Fig. 2.

For the waveguide cavity cross-coupled filters, the design method, which is based on deriving a coupling matrix from the transfer function and realizing the coupling matrix in terms of intercavity couplings, is widely used for its simplicity and accuracy [15] and [16]. It is thus desirable to adopt this synthesis technique to design cross-coupled microstrip square open-loop resonator filters. However, the application of such a design approach requires the knowledge of mutual couplings between coupled microstrip square open-loop resonators. This paper derives this information on mutual coupling.

Three basic coupling structures encountered in the type of cross-filters such as those in Fig. 1 are described in Section II. Because the semi-open configuration and inhomogeneous dielectric medium of the coupling structures make the associated boundary value problem complicated, a full-wave electromagnetic (EM) simulator is used to characterize the couplings in terms of resonant mode splitting. Section III

A. Electric Coupling

For the fundamental mode near its resonance, an equivalent lumped-element circuit model for the coupling structure in Fig. 2(a) is given in Fig. 3(a), where L and C are the self-inductance and self-capacitance so that $(LC)^{-1/2}$ equals the angular resonant frequency of uncoupled resonators, and C_m represents the mutual capacitance. At this stage it should be make clear that the coupled structure considered is inherently distributed element so that the lumped-element circuit equivalence is valid on a narrow-band basis, namely, near its resonance as we have emphasized at the beginning. The same comment is applicable for the other coupled structures discussed later. Now, if we look into reference planes $T_1 - T_1'$ and $T_2 - T_2'$, we can see a two-port network which may be described by the following set of equations

$$I_1 = j\omega C V_1 - j\omega C_m V_2 \tag{1a}$$

$$I_2 = j\omega C V_2 - j\omega C_m V_1 \tag{1b}$$

in which a sinusoidal waveform is assumed. It might be well to mention that (1a) and (1b) imply that the self-capacitance C is the capacitance seen in one resonant loop of Fig. 3(a) when the capacitance in the adjacent loop is shorted out. Thus, the second terms on the right-hand side of (1a) and (1b) are the induced currents resulted from the increasing voltage in resonant loop 2 and loop 1, respectively. From (1a) and (1b) four Y-parameters

$$Y_{11} = Y_{22}$$
$$= j\omega C \tag{2a}$$

$$Y_{12} = Y_{21}$$
$$= -j\omega C_m \tag{2b}$$

can easily be found by definitions.

According to the network theory [18] an alternative form of the equivalent circuit in Fig. 3(a) can be obtained and is shown in Fig. 3(b). This form yields the same two-port parameters with those of the circuit of Fig. 3(a), but it is more convenient for our discussions. Actually, it can be shown that the electric coupling between the two resonant loops is represented by an admittance inverter $J = \omega C_m$. If the symmetry plane $T - T'$ in Fig. 3(b) is replaced by an electric wall (or a short-circuit), the resultant circuit has a resonant frequency

$$f_e = \frac{1}{2\pi\sqrt{L(C + C_m)}}. \tag{3}$$

This resonant frequency is lower than that of uncoupled single resonator, which has also been confirmed by the full-wave simulations. A physical explanation is that the coupling effect enhances the capability of storing charge of the single resonator when the electric wall is inserted in the symmetrical plane of the coupled structure. Similarly, replacing the symmetry plane in Fig. 3(b) by a magnetic wall (or an open-circuit) results in a single resonant circuit having a resonant frequency

$$f_m = \frac{1}{2\pi\sqrt{L(C - C_m)}}. \tag{4}$$

In this case the coupling effect reduces the capability of storing charge so that the resonant frequency is increased.
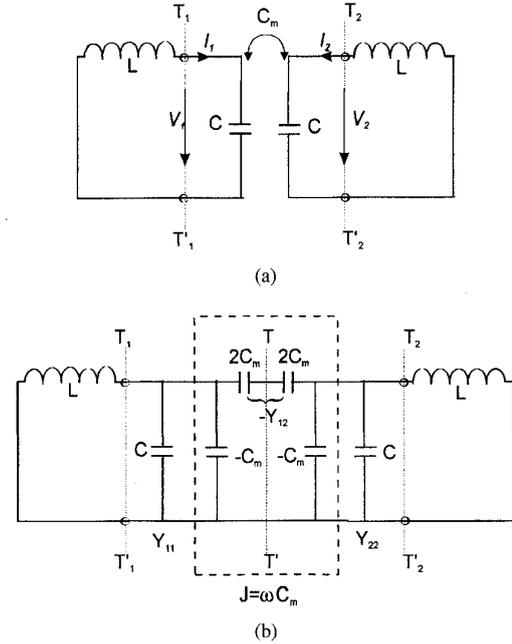

Fig. 3. (a) Equivalent circuit of the coupled open-loop resonators exhibiting the electric coupling. (b) An alternative form of the equivalent circuit with an admittance inverter $J = \omega C_m$ to represent the coupling.

Equations (3) and (4) can be used to find the electric coupling coefficient k_E

$$k_E = \frac{f_m^2 - f_e^2}{f_m^2 + f_e^2}$$
$$= \frac{C_m}{C} \tag{5}$$

which is identical with the definition of ratio of the coupled electric energy to the stored energy of uncoupled single resonator.

B. Magnetic Coupling

Shown in Fig. 4(a) is an equivalent lumped-element circuit model for the coupling structure in Fig. 2(b) near its resonance, where L and C are the self-inductance and self-capacitance, and L_m represents the mutual inductance. In this case the coupling equations described the two-port network at reference planes $T_1 - T_1'$ and $T_2 - T_2'$ are

$$V_1 = j\omega L I_1 + j\omega L_m I_2, \tag{6a}$$

$$V_2 = j\omega L I_2 + j\omega L_m I_1. \tag{6b}$$

Equations (6a) and (6b) also imply that the self-inductance L is the inductance seen in one resonant loop of Fig. 4(a) when the adjacent loop is open-circuited. Thus, the second terms on the right-hand side of (6a) and (6b) are the induced voltage resulted from the increasing current in loops 2 and 1, respectively. From (6a) and (6b) we can find four Z-parameters

$$Z_{11} = Z_{22}$$
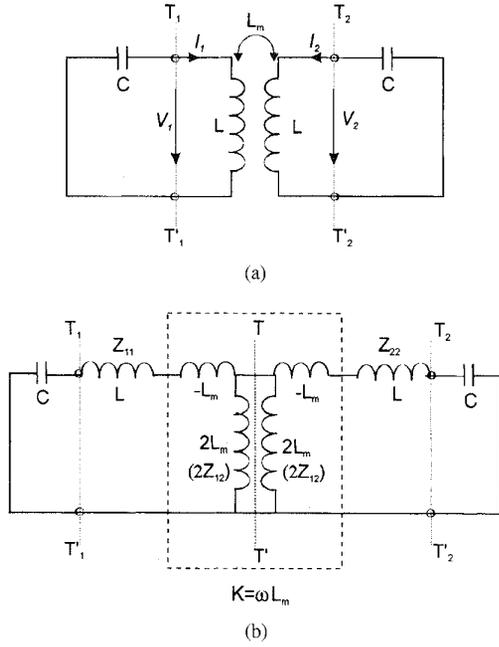$$= j\omega L, \tag{7a}$$

$$Z_{12} = Z_{21}$$

Fig. 4. (a) Equivalent circuit of the coupled open-loop resonators exhibiting the magnetic coupling. (b) An alternative form of the equivalent circuit with an impedance inverter $K = \omega L'_m$ to represent the coupling.

$$= j\omega L_m. \tag{7b}$$

Shown in Fig. 4(b) is an alternative form of equivalent circuits having the same network parameters as those of Fig. 4(a). Similarly, it can be shown that the magnetic coupling between the two resonant loops is represented by an impedance inverter $K = \omega L_m$. If the symmetry plane $T - T'$ in Fig. 4(b) is replaced by an electric wall (or a short-circuit), the resultant single resonant circuit has a resonant frequency

$$f_e = \frac{1}{2\pi\sqrt{(L - L_m)C}}. \tag{8}$$

It can be shown that the increase in resonant frequency, which has also been observed in the full-wave simulations, is because the coupling effect reduces the stored flux in the single resonator circuit when the electric wall is inserted in the symmetric plane. If the symmetry plane in Fig. 4(b) is replaced by a magnetic wall (or an open-circuit), the resultant single resonant circuit has a resonant frequency

$$f_m = \frac{1}{2\pi\sqrt{(L + L_m)C}}. \tag{9}$$

In this case it turns out that the coupling effect increases the stored flux so that the resonant frequency is shifted down.

Similarly, (8) and (9) can be used to find the magnetic coupling coefficient k_M

$$k_M = \frac{f_e^2 - f_m^2}{f_e^2 + f_m^2}$$
$$= \frac{L_m}{L}. \tag{10}$$

It should be emphasized that the magnetic coupling coefficient defined by (10) corresponds to the definition of ratio of the

coupled magnetic energy to the stored energy of uncoupled single resonator. One might also notice that the magnetic coupling defined by (10) and the electric coupling defined by (5) are in phase opposition. This type of coupling is what we really need for the realization of cross-coupled filters.

C. Mixed Coupling

For the coupling structure of Fig. 2(c), the electric and magnetic field distributions on the coupled arms of two resonators are comparative so that neither the electric coupling nor the magnetic coupling can be ignored. Hence, in this case the coupling may be referred to as the mixed coupling. For the fundamental mode of this coupling structure near its resonance, a network representation is shown in Fig. 5(a). Notice that the Y-parameters are the parameters of a two-port network looked into the left of reference plane $T_1 - T'_1$ and the right of reference plane $T_2 - T'_2$, while the Z-parameters are the parameters of the other two-port network looked into the right of reference plane $T_1 - T'_1$ and the left of reference plane $T_2 - T'_2$. The Y- and Z-parameters are defined by

$$
\begin{aligned}
Y_{11} &= Y_{22} \\
&= j\omega C, \\
Y_{12} &= Y_{21} \\
&= j\omega C'_m \\
Z_{11} &= Z_{22} \\
&= j\omega L, \\
Z_{12} &= Z_{21} \\
&= j\omega L'_m.
\end{aligned}
\tag{11}
$$
$$\tag{12}$$

where C, L, C'_m, and L'_m are the self-capacitance, the self-inductance, the mutual capacitance, and the mutual inductance of an associated equivalent lumped-element circuit shown in Fig. 5(b). It should be explained that the minus sign assigned to the mutual capacitance is based on two facts. The first fact is that the electric and magnetic couplings enhance each other (add in phase). The second fact is that when the symmetry plane of the equivalent circuit is shorted-circuit, which may correspond to the excitation for the currents on the coupled arms of Fig. 2(c) having the same magnitude but the opposite direction, the resonant frequency is higher than that of uncoupled single resonator. In Fig. 5(b), one can also identify an impedance inverter $K = \omega L'_m$ and an admittance inverter $J = \omega C'_m$ which represent the magnetic coupling and the electric coupling, respectively.

By inserting an electric wall and a magnetic wall into the symmetry plane of the equivalent circuit in Fig. 5(b), respectively, we obtain

$$f_e = \frac{1}{2\pi\sqrt{(L - L'_m)(C - C'_m)}}, \tag{13}$$

$$f_m = \frac{1}{2\pi\sqrt{(L + L'_m)(C + C'_m)}}. \tag{14}$$

As can be seen that both the magnetic and electric couplings have the same effect on the resonant frequency shifting. In other words, they reduce or enhance the stored flux/charge of
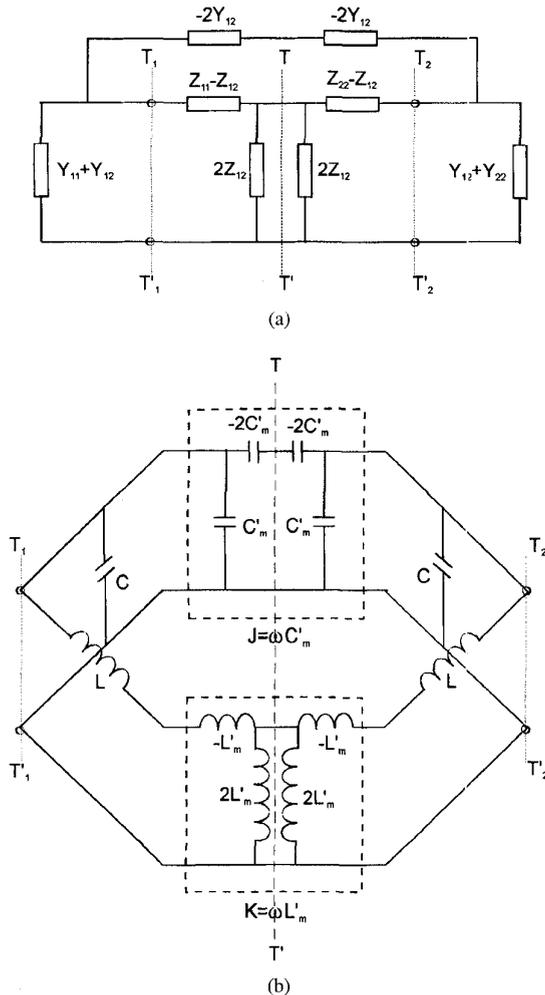
Fig. 5. (a) Network representation of the coupled open-loop resonators exhibiting the mixed coupling. (b) An associated equivalent circuit with an impedance inverter $K = \omega L'_m$ and an admittance inverter $J = \omega C'_m$ to represent the magnetic coupling and the electric coupling, respectively.

the single resonant circuit at the same time when the electric wall or the magnetic wall is inserted.

From (13) and (14) the mixed coupling coefficient k_B can be found to be

$$k_B = \frac{f_e^2 - f_m^2}{f_e^2 + f_m^2}$$
$$= \frac{CL'_m + LC'_m}{LC + L'_m C'_m}. \quad (15)$$

It is reasonable to assume that $L'_m C'_m \ll LC$, and thus (15) becomes

$$k_B \approx \frac{L'_m}{L} + \frac{C'_m}{C}$$
$$= k'_M + k'_E \quad (16)$$

which clearly indicates that the mixed coupling is resulted from the superposition of the magnetic and electric couplings, which are in phase, as would be expected.

IV. NUMERICAL COMPUTATIONS AND RESULTS

Before presenting any numerical results it should be remarked that for numerical computations, depending on the particular EM simulator used as well as the coupling structure analyzed, it may sometimes be difficult to implement the electric wall or the magnetic wall, or even the both in the simulation. For instance, the mixed coupling structure in Fig. 2(c) is actually symmetrical about a rotational axis rather than a plane. In this case, the difficulty can be removed easily by analyzing the whole coupling structure instead of the half, and finding the natural resonant frequencies of two resonant peaks observable from the resonant frequency response. It can be shown (see the Appendix) that the two natural resonant frequencies obtained in this way are f_e and f_m.

Shown in Fig. 6 are the typical resonant frequency responses of the three types of coupled open-loop resonators, which are obtained using a full-wave EM simulator based on the method of moments [19]. The two resonant peaks which correspond to the resonant frequencies f_e and f_m, defined above, are clearly identified. It can be seen that as the coupling spacing s decreases the two resonant peaks move outwards and the trough in the middle deepens, which implies an increase in the coupling. It would also seem that for the same coupling spacing the magnetic coupling is the strongest whereas the electric coupling is the weakest. From the information of resonant mode splitting the coupling coefficients can then be extracted using (5), (10), and (15) derived in the last section. The computed results give an insight into the characteristics of couplings and indicate that the couplings depend not only on the spacing but also on the other parameters.

Shown in Fig. 7 are the computed coupling coefficients for different dielectric constants of substrate. The electric coupling k_E shows a dependence of dielectric constant. The lower the dielectric constant, the stronger is the electric coupling. This is because the electric field is much confined in the substrate closer to the microstrip line having a higher dielectric constant. The numerical results also indicate that for low values of dielectric constant the variation of electric coupling with ε_r is rapid while it is rather slow for high values of ε_r. Again from Fig. 7 we can see that the magnetic coupling k_M clearly shows an independence of dielectric constant as what should be expected. While the mixed coupling k_B exhibits also a dependence on dielectric constant because it involves electric coupling. The width w of coupled open-loop arms (refer to Fig. 2) is another parameter on which the couplings depend. Fig. 8 shows the computed couplings vary with respect to w. It would seem that the couplings are stronger for a smaller w. The reason for this is because the fringe field is stronger for a narrow microstrip line. It is found that the couplings also depend on the size a of open-loop resonator (refer to Fig. 2). One can see in Fig. 9 that for the other parameters fixed the couplings increase as the size a increases. This phenomenon may also attribute to the increase in fringe field when a is increased. As stated above the coupled open-loop resonators may or may not be subject to an offset. Fig. 10 shows the computed coupling coefficients with and without the offset. As can be seen the magnetic and the mixed couplings do not change much against
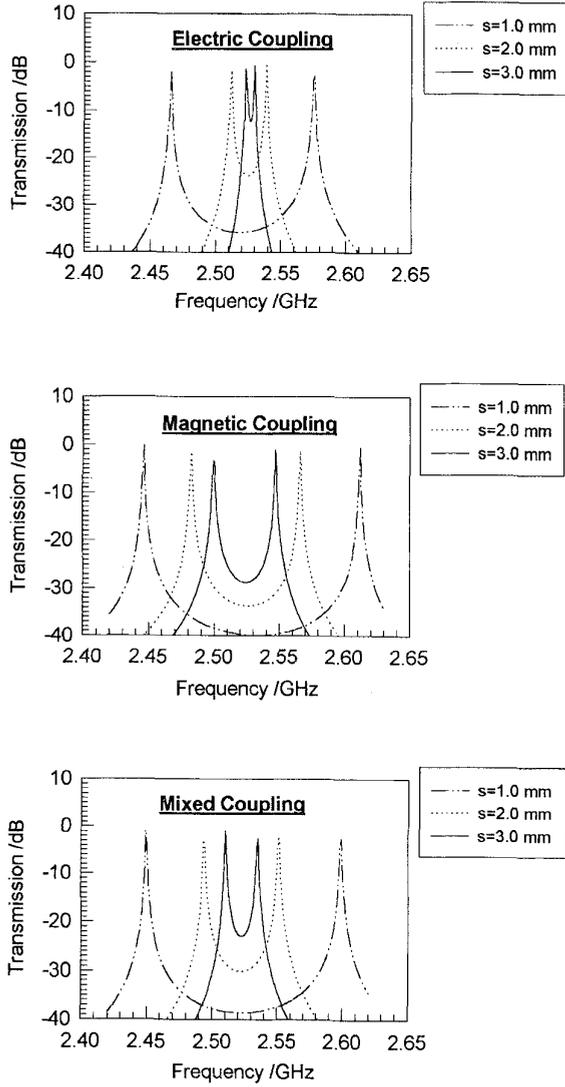
Fig. 6. Typical resonant mode splitting phenomena of the three types of coupled microstrip square open-loop resonators.

the offset d of the coupled resonators, whereas the electric coupling is more sensitive to the offset. For the filter realization the offset in electric coupling structure can actually be avoided.

It may be convenient for the filter design to estimate the couplings of coupled open-loop resonators using some closed formulas. It is found that for a given substrate with a relative dielectric constant ε_r and a thickness h, the coupling coefficients can be characterized in terms of normalized dimensions s/h, w/h, and a/h. By fitting the numerical results obtained above we find that the coupling coefficients may be fitted into the following models

$$k_E = \frac{\pi}{16} \cdot F_e \cdot \exp\left(-A_e\right) \cdot \exp\left(-B_e\right) \cdot \exp\left(-D_e\right)$$

$$A_e = 0.2259 - 0.015\,71\varepsilon_r + 0.1 \cdot \sqrt{\varepsilon_r + 1} \cdot \frac{w}{h}$$

$$B_e = \left[1.0678 + 0.266 \cdot \ln\left(\frac{\varepsilon_r + 1}{2}\right)\right] \cdot \left(\frac{s}{h}\right)^{pe},$$

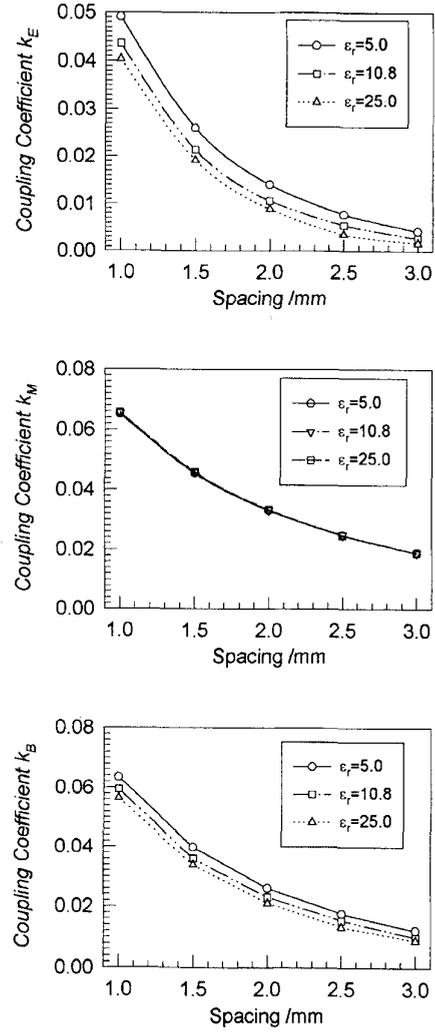$$pe = 1.0886 + 0.031\,46\left(\frac{w}{h}\right)^4$$

Fig. 7. Coupling coefficients for resonators with $a = 7.0$ mm, $w = 1.0$ mm, and $d = 0.0$ mm on a substrate with a thickness $h = 1.27$ mm and different relative dielectric constants.

$$D_e = \left[0.1608 - 0.069\,45\sqrt{\frac{a}{h}}\right] \cdot \left(\frac{s}{h}\right)^{1.15}$$

$$F_e = \left[-0.9605 + 1.4087\sqrt{\frac{a}{h}} - 0.2443\,\frac{a}{h}\right] \quad (17)$$

for the electric coupling coefficient

$$k_M = \frac{\pi}{16} \cdot F_m \cdot \exp\left(-A_m\right) \cdot \exp\left(-B_m\right) \cdot \exp\left(-D_m\right)$$

$$A_m = \left[-0.068\,34 + 0.141\,42\,\frac{w}{h} + 0.086\,55\left(\frac{w}{h}\right)^3\right]$$

$$B_m = 1.2 \cdot \left(\frac{s}{h}\right)^{pm},$$

$$pm = 0.8885 - 0.1751\sqrt{\frac{w}{h}}$$

$$D_m = \left[1.154 - 0.8242\sqrt{\frac{a}{h}} + 0.1417\,\frac{a}{h}\right] \cdot \left(\frac{s}{h}\right)$$

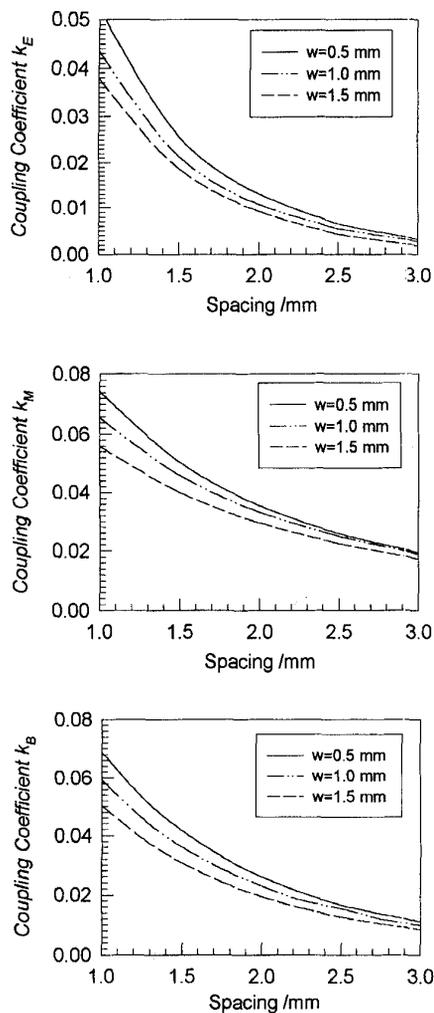$$F_m = -0.5014 + 1.0051\sqrt{\frac{a}{h}} - 0.1557\,\frac{a}{h} \quad (18)$$

Fig. 8. Coupling coefficients for coupled resonators with $a = 7.0$ mm, $d = 0.0$ mm and different w on a substrate of $\varepsilon_r = 10.8$ and thickness $h = 1.27$ mm.
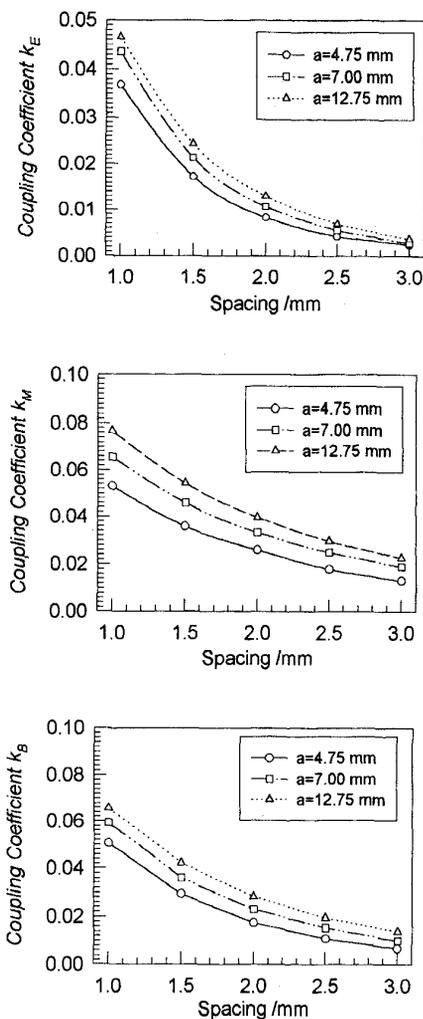
Fig. 9. Coupling coefficients for coupled resonators with $w = 1.0$ mm, $d = 0.0$ mm and different size a on a substrate of $\varepsilon_r = 10.8$ and thickness $h = 1.27$ mm.

for the magnetic coupling coefficient, and

$$k_B = k'_M + k'_E$$
$$k'_M = 0.5k_M$$
$$k'_E = 0.6k_E \tag{19}$$

for the mixed coupling coefficient. Shown in Fig. 11 are the coupling coefficients modeled by (17)–(19). Compared with the simulated ones obtained by the full-wave simulation, an accuracy better than 10% is achieved. The empirical formula of (19) is able to demonstrate quantitatively that the magnetic coupling is predominant in the mixed coupling case even though both the electric and magnetic couplings occur. As an example Fig. 12 plots the ratio of the electric coupling to the magnetic coupling in a mixed coupling structure on a substrate with a relative dielectric constant $\varepsilon_r = 10.8$ and a thickness $h = 1.27$ mm. As can be seen the electric coupling is less than 80% of the magnetic coupling, and the ratio is even smaller as

the spacing is increased because the electric coupling decays faster than the magnetic coupling against the spacing.

The full-wave EM simulator used has been proved to be quite accurate in its prediction. Nevertheless, a set of microstrip coupled open-loop resonators in Fig. 2 having a spacing 2.0 mm on a RT/Duroid substrate with $\varepsilon_r = 10.8$ and a thickness $h = 1.27$ mm were fabricated and measured to verify the theory. The measured coupling coefficients together with those obtained from the full-wave simulations and the closed-formulas are listed in Table I for comparison. Good agreement are obtained.

V. FILTER APPLICATIONS

A four-pole elliptic function bandpass filter is used to demonstrate the filter applications of the coupled microstrip square open-loop resonators. The center frequency of the filter is 2.46 GHz and the fractional bandwidth is 4%. The coupling matrix and input/output singly loaded $Q = 1/R$ to be realized
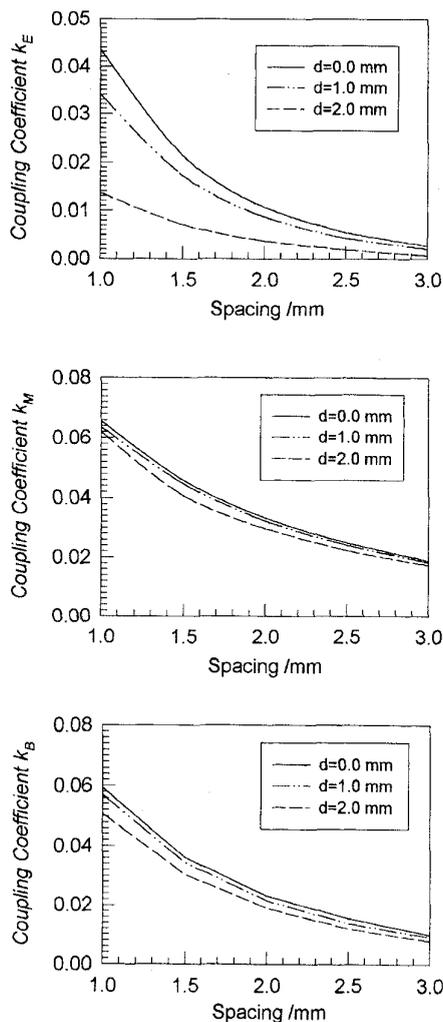
Fig. 10.   Coupling coefficients of the three types of coupled microstrip square open-loop resonators with $a = 7.0$ mm, $w = 1.0$ mm and different offset d on a substrate of $\varepsilon_r = 10.8$ and thickness $h = 1.27$ mm.

Fig. 11.   Comparison of the coupling coefficients modeled using the closed formulas to those simulated using the full-wave EM simulator.

are

$$M = \begin{bmatrix} 0 & 0.0261 & 0 & -0.0029 \\ 0.0261 & 0 & 0.022 & 0 \\ 0 & 0.022 & 0 & 0.0261 \\ -0.0029 & 0 & 0.0261 & 0 \end{bmatrix}$$

$$R = 0.035\,01. \tag{20}$$

The positive couplings $M_{12} = M_{21} = M_{34} = M_{43}$ and $M_{23} = M_{32}$ are realized by the mixed and magnetic couplings, respectively, while the negative coupling $M_{14} = M_{41}$ are realized by the electric coupling. The input/output loads are achieved via tapped feed lines [20]. Fig. 13(a) shows the layout of the filter and the frequency responses computed by an ideal circuit model. The filter was fabricated on a RT/Duroid substrate with a relative dielectric constant of 10.8 and a thickness of 1.27 mm. The measured filter performance is given in Fig. 13(b). The passband insertion loss is about 2.2 dB. This is mainly due to the conductor loss for a measured resonator Q of 200.
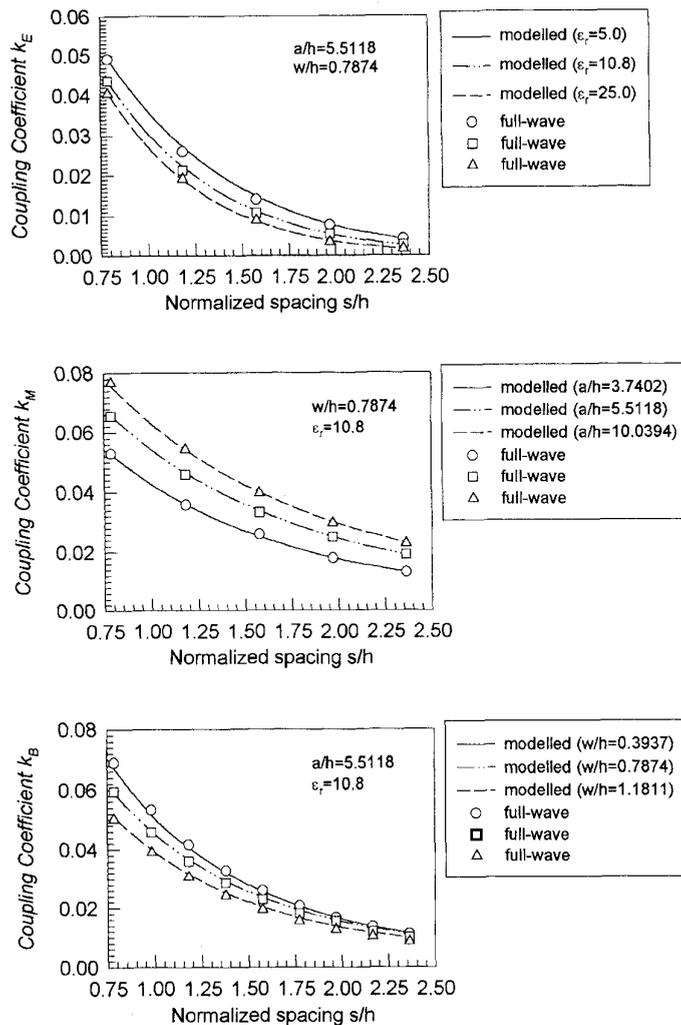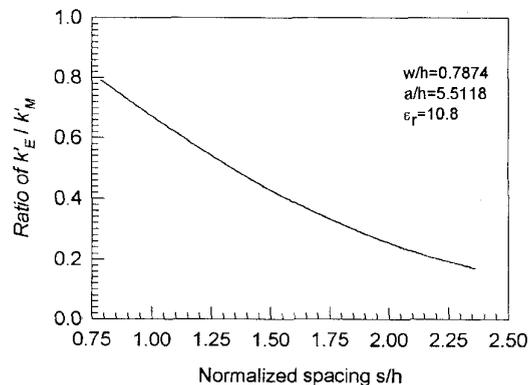
Fig. 12.   Ratio of the electric coupling to the magnetic coupling in the mixed coupling structure, showing the magnetic coupling is predominant.

VI. CONCLUSION

We have proposed a new type of planar cross-coupled filters using coupled microstrip square open-loop resonators. In order to apply the design technique which is widely used for the

TABLE I
COUPLING COEFFICIENTS OF COUPLED MICROSTRIP SQUARE OPEN-LOOP
RESONATORS ($\varepsilon_r = 10.8$, $h = 1.27$ mm, $w = 1.0$ mm, $s = 2.0$ mm)

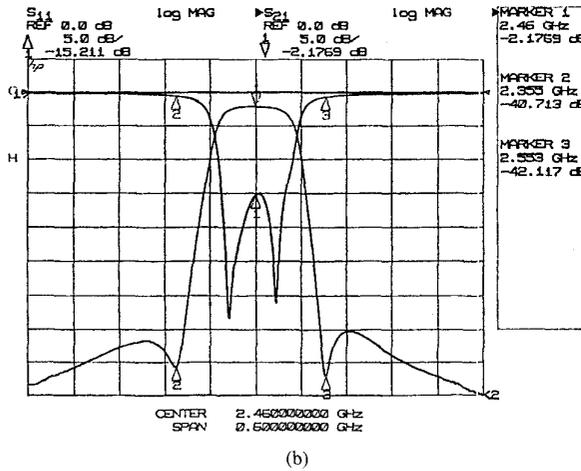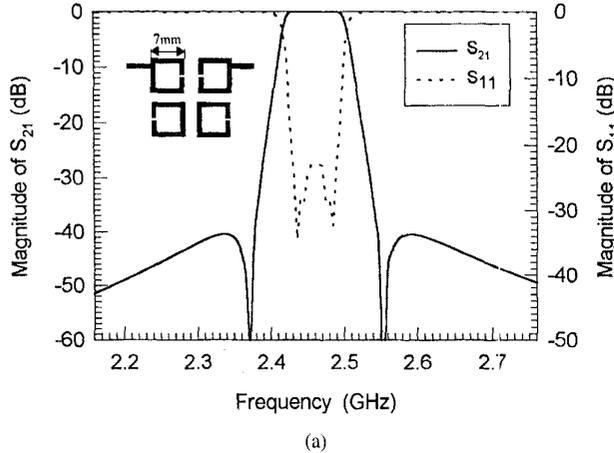| Type of coupling	Measured	Simulated	Modelled
Electric coupling	0.010	0.011	0.011
Magnetic coupling	0.031	0.033	0.034
Mixed coupling	0.023	0.023	0.024

(a)

(b)

Fig. 13. (a) Filter layout and performance of the ideal model for the four-pole filter. (b) Measured filter performance.

waveguide cavity filters to the proposed type of microstrip filters, a method for the rigorous calculation of the coupling coefficients of the three basic coupling structures encountered has been developed. We have presented the numerical results of the coupling coefficients obtained using full-wave EM simulations. The characteristics of the three types of couplings, namely the electric, magnetic and mixed couplings have been investigated. We have also derived three simple empirical modes for estimation of the coupling coefficients of these types of couplings. We have performed the experiments to verify the numerical results. To demonstrate the filter application, we have designed and fabricated a four-pole elliptic function filter of this type. Both theoretical and experimental performances of the filter have been presented.

APPENDIX
PROVE THAT f_e AND f_m ARE TWO NATURAL RESONANT FREQUENCIES

It would seem that the best way to show that f_e and f_m are the two natural resonant frequencies of the coupling structures in Fig. 2 is to prove that f_e and f_m are the two eigen values of the eigen equation in association with the individual coupling structure. For our purpose Fig. 14 shows the modified equivalent circuits of the three coupling structures of Fig. 2, where the resonators are all assumed tuned to the normalized center frequency $\omega_o = 1/\sqrt{LC} = 1$ and to have normalized characteristic impedance $z_o = \sqrt{L/C} = 1$. Thus the mutual capacitance and inductance are normalized to C and L, respectively. By deriving the Z-matrix of each equivalent circuit in Fig. 14 and imposing the boundary conditions $V_1 = V_2 = 0$ for natural resonance, the eigen equation can be found to be

$$Z_{11} \cdot Z_{22} - Z_{12} \cdot Z_{21} = 0. \tag{21}$$

For the electric coupling circuit we have

$$
\begin{aligned}
Z_{11} &= Z_{22} \\
&= \frac{A}{B}, \\
Z_{21} &= Z_{12} \\
&= \frac{1}{B}, \\
A &= 1 + \frac{1 - C_m}{C_m} - \omega^2 \cdot \frac{(1 - C_m)(1 + C_m)}{C_m}, \\
B &= j\omega \frac{(1 - C_m)(1 + C_m)}{C_m}.
\end{aligned}
\tag{22}
$$

With the normalized frequencies $\omega = 2\pi \cdot f_e = 1/\sqrt{1 + C_m}$ and $\omega = 2\pi \cdot f_m = 1/\sqrt{1 - C_m}$ of (3) and (4) defined in Section III, (21) is satisfied. This proves that f_e and f_m are indeed the two eigen values or the two natural resonant frequencies of the coupling structure of Fig. 2(a) regardless whether or not the electric or the magnetic wall is inserted.

For the magnetic coupling circuit we have

$$
\begin{aligned}
Z_{11} &= Z_{22} \\
&= \frac{A}{B}, \\
Z_{21} &= Z_{12} \\
&= \frac{1}{B}, \\
A &= 1 + \frac{(1 - L_m) - \dfrac{1}{\omega^2}}{L_m}, \\
B &= \frac{1}{j\omega L_m}.
\end{aligned}
\tag{23}
$$

Similarly, the eigen equation of (21) is satisfied with the normalized frequencies $\omega = 2\pi \cdot f_e = 1/\sqrt{1 - L_m}$ and $\omega = 2\pi \cdot f_m = 1/\sqrt{1 + L_m}$ of (8) and (9) given in Section III, indicating that f_e and f_m are the two eigen values or the two natural resonant frequencies of the coupling structure of Fig. 2(b) despite if the electric/magnetic wall is implemented or not.

Electric Coupling

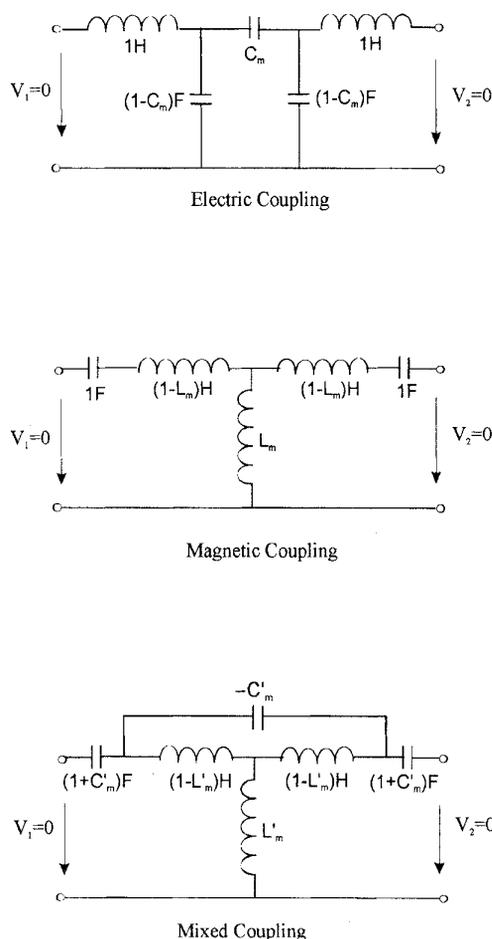Magnetic Coupling

Mixed Coupling

Fig. 14. Normalized equivalent circuits of the electric, the magnetic, and the mixed coupling structures for deriving the eigen equation of the coupled resonator circuit.

For the mixed coupling circuit we have

$$Z_{11} = Z_{22}$$
$$= \frac{Z_{11e} + Z_{11o}}{2},$$
$$Z_{21} = Z_{12}$$
$$= \frac{Z_{11e} - Z_{11o}}{2},$$
$$Z_{11e} = \frac{1 - \omega^2(1 + L_m')(1 + C_m')}{j\omega(1 + C_m')},$$
$$Z_{11o} = \frac{1 - \omega^2(1 - L_m')(1 - C_m')}{j\omega(1 + C_m')[1 + 2\omega^2 C_m'(1 - L_m')]}. \quad (24)$$

As can be seen $Z_{11o} = 0$ for the normalized frequency $\omega = 2\pi \cdot f_m = 1/\sqrt{(1 - L_m')(1 - C_m')}$ of (13) and $Z_{11e} = 0$ for the normalized frequency $\omega = 2\pi \cdot f_e = 1/\sqrt{(1 + L_m')(1 + C_m')}$ of (14) so that, again, (21) is satisfied, which give a proof that f_e and f_m defined by (13) and (14) are the two eigen values or the two natural resonant frequencies of the coupling structure of Fig. 2(c) without inserting the electric wall or the magnetic wall.

REFERENCES

[1] S. Darlington, "Synthesis of reactance four poles which produce prescribed insertion loss characteristics," *J. Math. Phys.*, vol. 18, pp. 257–353, Sept. 1939.

[2] R. Levy and S. B. Cohn, "A history of microwave filter research, design, and development," *IEEE Trans. Microwave Theory Tech.*, vol. MTT-32, pp. 1055–1067, Sept. 1984.

[3] J. A. Curtis and S. J. Fiedziuszko, "Miniature dual mode microstrip filters," in *IEEE MTT-S, Dig.*, 1991, pp. 443–446.

[4] _____, "Multi-layered planar filters based on aperture coupled dual mode microstrip or stripline resonators," in *IEEE MTT-S Dig.*, 1992, pp. 1203–1206.

[5] G. L. Matthaei and G. L. Hey-Shipton, "Novel staggered resonator array superconducting 2.3 GHz bandpass filter," in *IEEE MTT-S Dig.*, June 1993, pp. 1269–1272.

[6] S. J. Hedges and R. G. Humphreys, "An extracted pole microstrip elliptic function filter using high temperature superconductors," in *Proc. Eur. Microwave Conf.*, 1994, pp. 517–521.

[7] M. Sagawa, K. Takahashi, and M. Makimoto, "Miniaturized hairpin resonator filters and their application to receiver front-end MIC's," *IEEE Trans. Microwave Theory Tech.*, vol. 37, pp. 1991–1997, Dec. 1989.

[8] M. Makimoto, "Microstripline split-ring resonators and their application to bandpass filters," *Electronics and Communication in Japan.* New York: Wiley, 1989, vol. 12, no. 5, pt. 2, pp. 104–112.

[9] J. S. Hong and M. J. Lancaster, "Realization of quasielliptic function filter using dual-mode microstrip square loop resonators," *Elec. Lett.*, vol. 31, pp. 2085–2086, 1995.

[10] S. J. Yao, R. R. Bonetti, and A. E. Williams, "Generalized dual-plane multicoupled line filters," *IEEE Trans. Microwave Theory Tech.*, vol. 41, pp. 2182–2189, Dec. 1993.

[11] R. R. Bonetti and A. E. Williams, "New design techniques for coupled line filters with transmission zeros," in *Proc. Eur. Microwave Conf.*, 1993, pp. 240–243.

[12] J. S. Hong and M. J. Lancaster, "Microstrip bandpass filter using degenerate modes of a novel meander loop resonator," *IEEE Microwave Guided Wave Lett.*, vol. 5, pp. 371–372, 1995.

[13] _____, "Canonical microstrip filter using square open-loop resonators," *Elec. Lett.*, vol. 31, pp. 2020–2022, 1995.

[14] C. Rauscher, "Microwave channelized active filters—A new modular approach to achieving compactness and high selectivity," *IEEE Trans. Microwave Theory Tech.*, vol. 44, pp. 122–132, Jan. 1996.

[15] A. E. Atia and A. E. Williams, "Narrow-bandpass waveguide filters," *IEEE Trans. Microwave Theory Tech.*, vol. MTT-20, pp. 258–265, Apr. 1972.

[16] A. E. Atia, A. E. Williams, and R. W. Newcomb, "Narrow-band multiple-coupled cavity synthesis," *IEEE Trans. Circ. Sys.*, vol. CAS-21, pp. 649–655, Sept. 1974.

[17] B. I. Bleaney and B. Bleaney, *Electricity and Magnetism*, 3rd ed. Oxford: Oxford Univ. Press, 1976, vol. 1, ch. 7.

[18] C. G. Montgomery, R. H. Dicke, and E. M. Purcell, *Principles of Microwave Circuits.* New York: McGraw-Hill, 1948, ch. 4.

[19] EM User's Manual. Sonnet Software, Inc., Version 2.4, 1993.

[20] J. S. Wong, "Microstrip tapped-line filter design," *IEEE Trans. Microwave Theory Tech.*, vol. MTT-27, pp. 44–50, Jan. 1979.

Jia-Sheng Hong (M'94) received the D.Phil. degree in engineering science from Oxford University, U.K., in 1994. In 1983, he was awarded a Friedrich Ebert Scholarship.

From 1979 to 1983, he worked at Fuzhou University, China, as a Teaching/Research Assistant in radio engineering. He visited Karlsruhe University, Germany, where he worked on microwave and millimeter-wave techniques from 1984 to 1985. In 1986, he returned to Fuzhou University as a Lecturer in microwave communications. In 1990, he was awarded a K. C. Wong Scholarship by Oxford University and became a graduate member of St. Peter's College at Oxford University, where he conducted research in electromagnetic theory and applications. Since 1994, he has been a Research Fellow at Birmingham University, U.K. His current interests include RF and microwave devices for communications, antennas, microwave applications of high temperature superconductors, electromagnetic modeling, and the genetic approach for signal processing and optimization.

Michael J. Lancaster (M'94) received the degree in physics from Bath University, U K., in 1980. He received the Ph.D. degree in 1984 for research into nonlinear underwater acoustics.

He joined the surface acoustic wave (SAW) group at the Department of Engineering Science at Oxford University as a Research Fellow. The research was in the design of new, novel SAW devices, including filters and filter banks. These devices worked in the frequency range 10 MHz–1 GHz. In 1987, he became a Lecturer at The University of Birmingham in the School of Electronic and Electrical Engineering, lecturing in electromagnetic theory and microwave engineering. Shortly after he joined the school, he began the study of the science and applications of high temperature superconductors, working mainly at microwave frequencies. Currently, he heads the Electronic and Materials Devices group as a Reader. His present personal research interests include microwave filters and antennas, as well as the high frequency properties and applications of a number of novel and diverse materials.